IEEE Access
Multidisciplinary | Rapid Review | Open Access Journal

Received September 3, 2018, accepted September 18, 2018, date of publication October 8, 2018, date of current version October 29, 2018.

Digital Object Identifier 10.1109/ACCESS.2018.2872933

Design Concept and Development of a New Spherical Attitude Stabilizer for Small Satellites

SAJJAD KESHTKAR[1], JAIME A. MORENO[2], (Member, IEEE), HIROHISA KOJIMA[3], (Member, IEEE), AND EUSEBIO HERNÁNDEZ[4]

[1]School of Engineering and Science, Tecnológico de Monterrey, Altamira 89600, Mexico
[2]Instituto de Ingeniería, Universidad Nacional Autónoma de México, Mexico 04510, Mexico
[3]Department of Aeronautics and Astronautics, Tokyo Metropolitan University, Hino 191-0065, Japan
[4]Instituto Politécnico Nacional, ESIME Ticoman, Mexico 07340, Mexico

Corresponding author: Sajjad Keshtkar (skeshtkar@itesm.mx)

This work was supported by the DEGAPA-UNAM and Grants SEP-CONACyT N. 251552 and AEM-CONACyT N. 262887.

ABSTRACT This paper presents the description, design concept, and dynamics of a new control moment gyroscope with a spherical rotor, referred to here as a spherical stabilizer. This stabilizer can be used as an alternative low-weight and high-precision triaxial attitude control device for small and experimental satellites. The mechanical design, as well as precision and structural analysis of the mechanism, is studied in detail. A numerical example of a specific satellite is presented and a fatigue simulation using the finite element method is carried out to examine the failure behavior of critical parts of the mechanism. The performance of the proposed mechanism as attitude controller of a small satellite is also studied via numerical simulations.

INDEX TERMS Control moment gyroscope, spherical stabilizer, friction drive, satellite's attitude control.

NOMENCLATURE

A_1, A_2, A_3	point on the intersection of the imaginary axis and the sphere
a, a_{per}	distance and permissible distance between axes of rotors
D_1, D_s	diameter of the driving wheel and sphere
E	elasticity modulus
f	friction coefficient
F_f, F_t, F_p	friction, effective and pressing forces
$\mathbf{H}$	kinetic moment of the rotor
i	transmission ratio
I_s	inertia moment of the sphere
J_x, J_y, J_z	inertia moment of the satellite
k_i, κ_i	controller gains
K	coupling reserve
m	mass of rotor
K	coupling reserve
$\mathbf{M}_c, \mathbf{M}_p$	controlling and perturbing torques
$Oxyz$	main axes of the rotor
R_{in}	magnitude correlating the kinetic energy to the mass of rotors
T, T_s, T_f	kinetic energies
v_*	the instantaneous orbital angular velocity
v_x, v_y, v_z	relative linear velocities of the rotor
λ	coefficient relating the vectors of angular velocity and kinetic energy
ω, ϖ	angular velocity of the rotor and satellite
$\Omega_{x,y,z}$	Euler angles of satellite rotation
$\omega_x, \omega_y, \omega_z$	projections of the angular velocities of the rotor
ρ_E	the radius vector of a point in Euler's formula
$\varrho, \rho, \rho_f, \rho_s$	dimensionless parameters for analyzing the characteristics of the rotors
τ_x, τ_y, τ_z	torques of motors
σ_t	contact stress

I. INTRODUCTION

Conventionally the control moments for precise triaxial attitude control of small satellites are created by momentum exchange devices. This is the best option for the microsatellites (less than 100 kg) which are usually transported to orbit as secondary payloads and are not permitted to carry their own working fluid. The growing demand for low-cost microsatellites and the upcoming deployment of LEO mega-constellations with high requirements on precision attitude control and pointing will likely increase the need for development of high performance and low weight attitude control devices [1], [2].

The reaction wheels and control moment gyros are the most well-known momentum exchange devices studied widely by the researchers [3]–[5]. Evidently, to create control moments with respect to all three stabilizing axes at least either three reaction wheels or three single gimbal gyroscopes are required [3], [6]. The stabilizing devices with these architectures are usually heavy and spacious and may cause singularities in the control system. Although Kwon *et al.* [7], Takehana *et al.* [8], and Kojima *et al.* [9] proposed (with some restrictions) designs with just two single gimbal control moment gyros and some others have proposed the miniaturized designs [10], [11] but these devices are still not optimal for small satellites due to their heavy and relatively spacious structure.

A perspective inertial actuator which is able to accelerate the satellite about any arbitrary axis is the control momentum device with spherical rotor known also as reactions spheres. By spinning a spherical rotor around its center (a point) with the regulated velocity and direction the necessary controlling torques can be created. This concept has several advantages over the classical momentum devices:

- its symmetrical shape allows to control the angular movements of the satellite simultaneously around all three axes;
- the spherical wheel is not gyroscopically connected to the body of the apparatus, and as a result, there is no gyroscopic connection between the control axes in the control system and the wheel;
- elimination of the singularity in the control system;
- full weight and volume advantage and simplicity of control structure due to the fact that only one reaction mass (one sphere) is used.

Although the idea of reaction spheres was proposed more than five decades ago [12], [13], due to the technological complicity their implementation was not introduced until recently. The main reason for increasing the interest in these devices is the tendency to miniaturize the attitude control units and advanced technologies in electronics. In recent years, many researches were dedicated to the design and application of these mechanisms. The major differences in these proposals consist of the driving and supporting strategies. Induction [14]–[16], permanent magnets [17]–[19] and hysteresis [20], [21] based motors are the main proposed types of driving and torque generation principles methods. The common bearing types are classified into electrostatic bearing, induction bearing, electrostatic bearing, active and permanent magnet bearing and air bearing. Although they have some differences, the main idea is the contactless rotating and a suspension of the sphere. The reason is to eliminate the friction and wear issues and avoid possible mechanical failures in an assembly with high rotation speed.

The idea of applying the reaction spheres for small satellites has been also of interest and many researches and projects are addressing the issue (see for example [15], [18]). Despite the efforts and active researchers here is no real application of these mechanisms out of the experimental labs. The main reason is that the stator of these devices is not efficient enough yet which leads to the increase in their size and weight (several times bigger than those of the spherical rotor). For instance in case of inductive reaction sphere with magnetization suspension in [15] to rotate a sphere with a diameter of 100 mm and a mass of 3.45 kg by speed of 13,500 in one direction four driving coils' core with dimensions $40\times40\times90$ mm^3, excluding the wires and power units was used. In fact the best dimensional ratio between the rotor and total device was reported in [18] where the permanent magnet stator has a diameter triple larger than that of the reaction sphere [22].

Piezoelectric and ultrasonic motors which transfer the electrical energy into high-frequency mechanical vibrations and transmit to the rotor by friction are studied by Paku and Uchiyama [23], Bakanauskas *et al.* [24]. In spite of the fact that by using this method a compact reaction with sphere/device dimension ratio (1/1.7 in [23]) can be obtained, due to their low velocity and high power consumption they did not find a wide application in attitude control of satellites.

In order to eliminate the mentioned disadvantages high-efficiency DC motors can be used alternatively. For instance, the coreless DC motors with small mass can reach high torques and consume less energy and, thus, have been widely used in the space applications. Although the use of these motors as the driver has been proposed [8], [25] and the possibilities and theoretical properties of this mechanism have been studied, there is not still a clear and functional mechanical design and detailed structural analysis for a practical use. The model presented in [8] and [23] does not have a removing mechanism, which disconnects the motor from the sphere after actuation, and hence suffers a big friction and can just produce torques in two directions.

In what follows, we present a detailed mechanical development and new design of a spherical control moment gyroscope which is compact and power optimized enough and therefore suitable to be used in real space missions. It would be shown in an example that a low rotor/device dimension and weight ratio can be easily obtained by use of an efficient transmitting mechanism. Despite the fact that such a mechanism can suffer from high contact stress and damage in a long time, this is still a suitable option for experimental and low-cost satellites whose active life does not exceed just a couple of years.

II. MODEL DESCRIPTION AND MATHEMATICAL MODEL

A. GENERAL DESCRIPTION OF THE MECHANISM

The spherical gyroscope as a satellite stabilizer can be interpreted as a rotor of a motor, the stator of which is the spacecraft (with the consideration that the supporting structure of the rotor is rigidly connected to the body of the satellite). When the rotor starts to spin, the satellite starts to rotate in the opposite direction, obeying the known law of action and reaction. In the proposed design, as it is schematically depicted in the Fig. 1, the inertial rotor (sphere) is held with

eight rolling elements installed in a spherical case. Six electric motors are situated in three orthogonal surfaces and each counter-position pair of motors creates a regulable torque that further is transmitted to the sphere by friction drive and spins the rotor on the corresponding surface. The driving wheels are detached from the sphere in the nonfunctional state and the consecutive activation of the motors and connection of the friction drives to the sphere provides its rotation around any arbitrary axis (which passes through its mass center) and, consequently, the creation of evenly controlling torque in any direction.

The detailed design of the structural parts, transmission part and the sliding mechanism for switching-in and removing of the friction drive with the spherical rotor will be presented in the next sections.

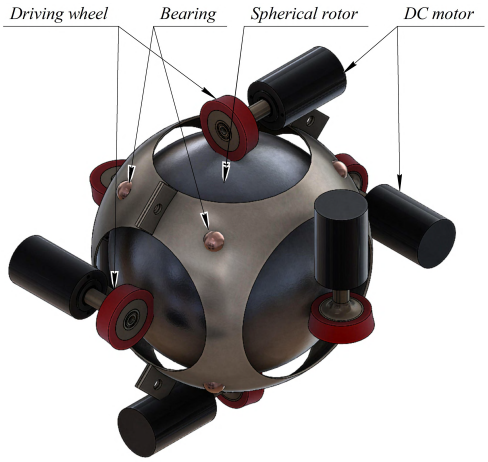

FIGURE 1. Schematic representation of main parts of the spherical stabilizer.

As it can be seen in the Fig 1, the rotor is not rigidly connected to the body of the satellite and, therefore, with its rotation, no gyroscopic moments occur in the spacecraft. The absence of these gyroscopic moments, which are usual phenomena in reaction wheels or control moment gyros, greatly facilitates the creation of a high-precision orientation system. On the other hand, the spherical gyroscopes have the advantage of a lighter mass compared to reaction wheels or gimbal control moment gyroscopes, where various actuators are needed for triaxial orientation of a satellite.

B. MATHEMATICAL MODEL OF THE SYSTEM

Assume that the geometrical center and the mass center of the rotor O' maintains motionless respect to the satellite. DC motors are situated on the surfaces that pass through the point O' and are parallel to the coordinate surfaces of axes $Oxyz$ (main axes of the satellite). In Fig. 2 the six arcs representing the actuators are conditionally pictured, where pairs *1* and *4*, *2* and *5*, *3* and *6* represent the stators of the six motors. In this case, the spherical rotor does not have any (principal) axes of spinning, therefore, the rotation of the sphere can be represented by any convenient projection of its

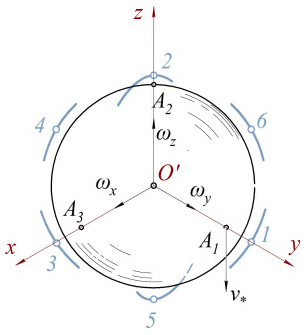

FIGURE 2. Spherical rotor of the proposed stabilizer.

angular velocity ω_s, for instance ω_x, ω_y, ω_z with respect to the main satellite coordinate system $Oxyz$.

The velocity and direction of rotation of the sphere can be estimated from the information of at least optical sensors [26] installed orthogonally above the sphere [8]. Suppose that the measurements show velocities v_x, v_y, v_z on the imaginary axes Ox, Oy, Oz on the corresponding points A_1, A_2, A_3, where the encoders are installed, with the coordinate systems on the $O'xyz$ axes

$$A_1(0, R, 0)^\top, \quad A_2(0, 0, R)^\top, \quad A_3(R, 0, 0)^\top \tag{1}$$

where R is the radius of the sphere. The field of relative linear velocities of the points of rotor can be defined by Euler's formula

$$\mathbf{v} = \boldsymbol{\omega}_s \times \rho_E, \tag{2}$$

where ρ_E is the radius-vector of the point, set from O'. From here

$$v_x = R\omega_x \quad v_y = R\omega_y \quad v_z = R\omega_z \tag{3}$$

i.e. the signals of sensors are proportional to ω_x, ω_y, ω_z, the projections of the angular velocity of the sphere $\boldsymbol{\omega}_s$. If the inertia ellipsoid of the rotor, as it should be in the ideal case, is a sphere, the kinetic moment of stabilizer can be obtained as

$$\mathbf{H} = I_s\boldsymbol{\omega}_s$$

where I_s is the inertia moment of the rotor with respect to any central axis. Consequently, the projections of the vector $\mathbf{H}$ on the axes $Oxyz$ are

$$H_x = I_s\omega_x \quad H_y = I_s\omega_y \quad H_z = I_s\omega_z \tag{4}$$

The bounded angular velocity of the sphere $\boldsymbol{\omega}_s$

$$|\omega_x|, \quad |\omega_y|, \quad |\omega_z| \le \omega_{max}, \tag{5}$$

creates a region of summary kinetic moment variation of the rotor, which can be conformed as a cube with edges equal to $2I_s\omega_{max}$ parallel to axes $Oxyz$.

The projection of controlling torque $\mathbf{M}'_c$ in the ideal case is directly proportional to the sum of active torques of motors

τ_x, τ_y, τ_z, of each par situated on the main axes of $Oxyz$. The projections of the moment $\mathbf{M}_c$ on the axes $Oxyz$ are

$$M'_{cx} = i\tau_x, \quad M'_{cy} = i\tau_y, \quad M'_{cz} = i\tau_z, \tag{6}$$

where $i > 0$ is the transmission ratio between the diameter of driving wheels connected to the motors and the diameter of the rotor. In reality, there are always perturbing torques $\mathbf{M}_p$ acting on the rotor such as inexact positioning of the sphere, moment of friction losses, additional active moments of DC motors, etc. The exact study of these moments requires a detailed research which is not provided in this work. Here we assume that the sum of all perturbations is bounded by

$$\|\mathbf{M}_{p_{x,y,z}}\| \leq L, \quad L > 0.$$

Suppose that the absolute kinetic moment of the sphere $\mathbf{H_s}$ for which

$$\dot{\mathbf{H}}_s = \mathbf{M}'_c, \tag{7}$$

is linked with its relative kinetic moment $\mathbf{H}$ with the expression

$$\mathbf{H_s} = I_s(\boldsymbol{\omega}_s + \boldsymbol{\varpi}) = \mathbf{H} + I_s\boldsymbol{\varpi} \tag{8}$$

where $\boldsymbol{\varpi}$ is the inertial angular velocity of the satellite. Therefore, the control torque generated by the stabilizer $\mathbf{M}_c$ can be calculated as

$$\mathbf{M}_c = -\dot{\mathbf{H}} = -\dot{\mathbf{H}}_s + I_s\dot{\boldsymbol{\varpi}} = -M'_c + I_s\dot{\boldsymbol{\varpi}}, \tag{9}$$

and with taking into account the perturbation forces, the complete control torque can be defined as

$$\begin{aligned} M_{cx} &= -i\tau_x - M_{p_x} + I_s\dot{\varpi}_x, \\ M_{cy} &= -i\tau_y - M_{p_y} + I_s\dot{\varpi}_y, \\ M_{cz} &= -i\tau_z - M_{p_z} + I_s\dot{\varpi}_z. \end{aligned} \tag{10}$$

In practice, the angular velocities ϖ and ω_s almost always hold the

$$\omega_s \gg \varpi. \tag{11}$$

In this case the following can be assumed

$$\mathbf{H} = \mathbf{H}_s \tag{12}$$

which simplifies the expressions of control torques of the stabilizer (10) to

$$\begin{aligned} M_{cx} &= -i\tau_x - M_{p_x}, \\ M_{cy} &= -i\tau_y - M_{p_y}, \\ M_{cz} &= -i\tau_z - M_{p_z}. \end{aligned} \tag{13}$$

C. DYNAMICAL PROPERTIES OF THE SPHERICAL STABILIZER

It can be seen that each expression of (13) has the same appearance as an expression of a torque created by a reaction wheel. In the general case with three orthogonally related reaction wheels, however, the torque created by a spherical stabilizer (13) has a simpler form. The reason is that the reaction wheels create additional gyroscopic torques in the surfaces perpendicular to the axis of their rotation and furthermore crossed terms appear [4]. In terms of simplicity of control design, the spherical stabilizer is superior to other momentum exchange devices and can be compared with the structure of the control torques created by a set of propulsion engines.

There are other parameters which can characterize the quality of one or another momentum exchange device and compare them. Some of the most important of these characteristics can be weight, energy-consumption, volume, and reliability. A simple analysis of the properties of an attitude control device which does not require the analysis of its construction and at the same time characterizes it from the viewpoint of creating kinematic moment $\mathbf{H}$, can be obtained by correlating the value H with the summery mass of rotors and a magnitude, which characterizes its relative angular velocity R_{in} around the rotating axis [25], [27]

$$R_{in} = \sqrt{H/m\omega} \tag{14}$$

If the dimensions of the rotor (radius R) are fixed, for the analysis of its characteristics a following dimensionless quantity can be used

$$\varrho = R_{in}^2/R^2 \leq 1. \tag{15}$$

For the case of multiple rotors the expressions (14) and (15) can be generalized with the following dimensionless parameter

$$\rho = H^2/2mTL^2,$$

where m is the total mass of all moving elements, participants in the creation of the kinetic moment H; T is their kinetic energy; L is any linear magnitude, defining the system of moving masses. Let us now compare the proposed scheme with a mechanism with three equal one-axis gyro stabilizer (reaction wheels) with rotation axes, parallel to the axes of satellite $Oxyz$. The Inertia moment of the sphere is

$$I_s = \frac{2}{5}m_sR_s^2,$$

where R_s is radius of sphere, m_s is its mass. For every of three flywheels

$$I_f = \frac{1}{2}m_fR_f^2,$$

that corresponds to a flywheel with mass m_f with a radius R_f. It is significant to mention that in the plane case one-axis flywheel has an advantage comparing with the spherical one, since

$$\frac{\rho_f}{\rho_s} = \frac{H_f^2/2mTR_f^2}{H_s^2/2mTR_s^2} = \frac{H_f^2I_f/H_f^2mR_f^2}{H_s^2I_s/H_s^2mR_s^2} = 5/4.$$

On the other hand in the triaxial case we have

$$\begin{aligned} H_s^2 &= I_s^2\left(\omega_x^2 + \omega_y^2 + \omega_z^2\right), \qquad 2T_s = H_s^2/I_s; \\ H_f^2 &= I_s^2\left(p_f^2 + q_f^2 + r_f^2\right), \qquad 2T_f = H_f^2/I_f, \end{aligned}$$

where p_f, q_f and, r_f are the projections of the angular velocity of the flywheels on the axes $Oxyz$; The parameter ρ for two comparing systems, taking L as the radius of sphere R_s in the first case and in the other case radius of one reaction wheel R_f, are

$$\rho_s = 2/5, \quad \rho_f = 1/6, \tag{16}$$

i.e. under this index, the spherical gyroscope in about two times surpasses the system with single-axis stabilizers.

This obtained result is due to the fact, that with any disposition of kinetic moment **H** respect to the axes $Oxyz$ all mass elements dm of the spherical gyroscope has linear velocities **v**, with respect to the vector **H**, and, consequently, in the best way take part in its creation. In the system with three reaction wheels with p_f, q_f, $r_f \neq 0$ practically each moving element dm has a component of linear velocity **v**, parallel to the vector **H**, which is useful for its creation.

Additionally, it has to be mentioned, that if in Eq. (16) one takes L as some parameter of the global dimensions of the system, then the system with three reaction wheels has to be taken as $L > R_f$ which makes ρ_s/ρ_f even greater. From this point of view, the superiority of spherical stabilizer with respect to one-axis gyro stabilizer with rotating mechanism also can be explained.

Although these analyses demonstrate clear weight and mathematical simplicity advantages of the spherical stabilizer, however, from the construction and reliability point of view, the actual designs of spherical stabilizers should still be improved to replace reaction wheels or control moment gyros.

III. CONCEPTUAL DESIGN OF ROTATION TRANSMISSION BY FRICTION DRIVES

In the proposed mechanism, the torques produced by the motors are transmitted to the spherical rotor by using friction drives. The rotation, in this case, can be transmitted from the driving shaft (motors) to the driven (sphere) by frictional forces, either by direct contact (transmission with rigid rolling bodies) or by using an intermediate link that can be rigid (for example, a steel ring) or flexible (belt, steel band, rope, chain with friction pads) [28], [29].

The main advantages of the friction drives are easy speed control of the driven shaft; simplicity of design and assembly; smooth motion and noiselessness. Due to the fact that the friction pair includes parts, with a real embodiment of the corresponding axoids in relative motion, it can provide the instantaneous value of the transmission ratio most accurately.

The kinematic scheme of the friction drive mechanism created by motors 1 and 4 along the y-axis is shown in Fig. 3. The transmission consists of the lead (driving) wheels 1, 4 and the driven sphere 2, as well as supports 3 and 5 which are designed to be automatically adjusted.

Friction drives inherent disadvantages: large pressures on shafts and supports due to use of friction forces in their work; the reliability of the transmission characteristics; low durability in high-pressure conditions; Geometric slip in the contact areas, reducing efficiency and service life of the drive.

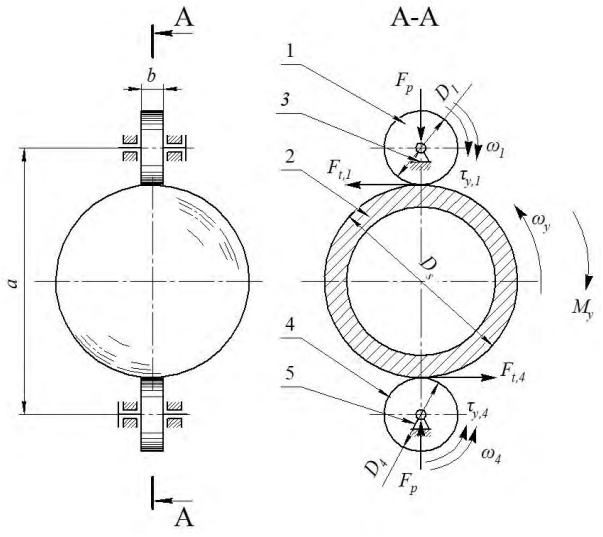

FIGURE 3. Schematic representation of friction drive in the active mode.

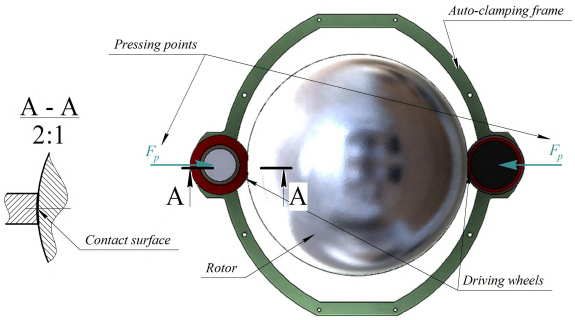

FIGURE 4. Solutions for friction drive improvement.

To eliminate or diminish these disadvantages the next design solutions are applied (Fig. 4):

1. Optimization of the friction pair form by conjugating the convex surface of the sphere with a concave shape driving wheels, which increases significantly the contact zone and, consequently, reduces the contact pressure.

2. Design of thick frames, which can be deformed after acting of the external forces. The energy of the work done is transferred and saved in the body, stores as potential energy. This potential energy, which is called the strain energy, gives auto-clamping properties to the frame and eliminates the need for additional clamping devices and increase the reliability of the system.

3. Use of two motors in each axis, which leads to a redundant and, therefore, more reliable design and allows to implement smaller and more compact motors.

4. Use of textolite [30] (a Composite Epoxy Material [31]) as the driving wheel material (instead of the proposed steel - steel pair in [8]). The textolite - steel pair can work without lubrication; they have a higher coefficient of friction than

steel and therefore work with the less pressing force. They are less demanding for the accuracy of the fabrication, assembly, and roughness of the working surfaces.

5. An automatic removal system for driving wheels which are activated only when a change in rotation velocity or the orientation of the spherical rotor is needed. As it is shown schematically in Fig. 5, the main shaft *5* of the driving wheel *7* and the support shaft *9* can slide between the toothed shaft *4* of the electric motor *1* and structure frame *8* and, consequently, transmit the rotation to the sphere *2*. The active and inactive modes are regulated by the spring *11* and electromagnet *10*. The frame *3* and bearing *6* are for fixing the electric motor and free rotation of the main shaft *5* accordingly.

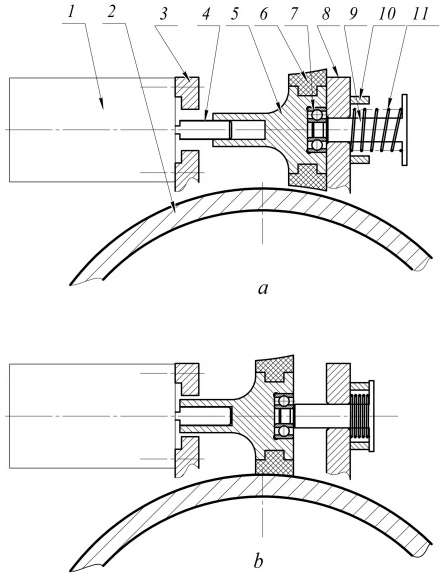

FIGURE 5. Design of support for automatic function of driving wheels.

A. MECHANICS OF THE TRANSMISSION

1) KINEMATICS OF THE TRANSMISSION

In frictional drives, because of the slippage and the elastic displacements of the contact points the circumferential speed of the driven wheel (sphere) is less than that of driving wheels and, as a consequence, the difference in the velocities at the points of the contact area.

The effect of slippage can be considered by coefficient ξ determined by [29]

$$\varepsilon = \frac{v_1 - v_y}{v_1}; \quad v_y = (1-\varepsilon)v_1,$$

where v_1 is the velocity of the wheel 1 (Fig. 3) and v_y is the velocity of the sphere in Oy-axis direction. The transmission ratio can be defined by the angular velocities of the driving wheel ω_1 and sphere ω_y of the rollers in Oy-axis,

$$i = \frac{\omega_1}{\omega_y} = -\frac{D_s}{(1-\varepsilon)D_1}, \tag{17}$$

For the textolite-steel pairing, the slip coefficient $\varepsilon = 0,01$; we assume that the angular velocities of $\omega_1 = \omega_4$.

2) STATICS OF THE TRANSMISSION

Suppose that a perturbation moment M_y which acts on the satellite in axis y should be compensated by the stabilizer, then to overcome this moment an effective force $F_{t,1}$ (generated by a pair of motors) is needed

$$F_{t,1} = M_y/D_s = F_f,$$

where F_f is the friction force, arising between contacting surfaces

$$F_f = fF_p$$

f is the friction coefficient for the steel-textolite pairing without lubrication $f = 0.2, \cdots, 0.25$.

To reduce the slippage during operation (due to wear, vibration, shifting, etc.), a coupling reserve is used $K = F_f/F_{t,1} > 0$. Usually, the coefficient is taken $K = 1.25, \cdots, 1.5$.

The required pressing force of the pairs is

$$F_p = \frac{KF_{t,1}}{f} = \frac{2KM_y}{fD_s}. \tag{18}$$

Pressing of the pairs is a necessary condition for the operation of the drive and the pressing method has a significant effect on the operation of the mechanism. The methods of pressing have become widespread: by means of special springs, by centrifugal forces and automatically under the action of the transmitted load. In the proposed mechanism the interference between the driving wheels and the sphere is used as a pressing method. Due to the flexibility of frames, they will have adjustable characteristics and, as a result, the transmission drive will have a longer operating life.

3) EFFICIENCY OF THE TRANSMISSION

$$\eta = M_{sy}\omega_y/(M_{ay,1}\omega_1 + M_{ay,4}\omega_4) = M_{sy}/M_{ay}i,$$

Losses in friction drives are caused by rolling friction between pairs, friction in bearings and lapping. Usually $\eta = 0.9 \sim 0.95$.

B. FUNCTIONALITY AND CALCULATION OF TRANSMISSION WHEELS

In the transmissions, without lubrication, the deterioration of driving wheel is widely observed. This deterioration is proportional to the maximum contact stress $q_{max} = \sigma_t$ generated by pressing force and friction coefficient f. The nonmetallic wheels can be destroyed due to flaking of the working surfaces. Accordingly, the contact strength and wear-resisting properties are the main criteria of the state of serviceability of the transmissions.

The contact strength calculation is carried out using the condition of strength reliability as [28] and [29]

$$\sigma_t \leq [\sigma_t] \tag{19}$$

where σ_t and $[\sigma_t]$ are accordingly the maximum and permissible contact stresses. For the friction pare textolite-steel pair it is established to take $[\sigma_t] = 50, \cdots, 70$.

For our case with curvature contact surfaces the stress can be determined by Hertz formula

$$\sigma_t = 0.418\sqrt{F_p E/2b\rho} \tag{20}$$

where b is the width of the contact between friction par; F_p is the pressing force of contacting bodies; E is so-called the modified modulus of longitudinal elasticity of friction pair materials, which with elasticity modulus E_1 and E_2 of first and second bodies, are defined as

$$E = 2E_1E_2/(E_1 + E_2) \tag{21}$$

$1/\rho$ is the modified curvature of working surfaces; for external contact of parallel rotary bodies

$$\frac{1}{\rho} = \frac{1}{\rho_1} - \frac{1}{\rho_s} = \frac{2}{D_1}\left(1 - \frac{D_1}{D_s}\right) \tag{22}$$

where D_1, D_s are diameters of the bodies 1, 2; the expressions for bodies 1 and 4 are the same.

The Eq. (19) then is transformed into

$$\sigma_t = 0.836\sqrt{\frac{KM_yE(i-1)}{2fD_s^2bi}} \le [\sigma_t], \tag{23}$$

or

$$\sigma_t = 0.418\sqrt{\frac{KM_yK(i-1)^3E}{2f(a/2)^2bi}} \le [\sigma_t], \tag{24}$$

where a is the distance between axes of leading rings 1, 4 (Fig. 3). Introducing the coefficient of width of driving wheels $\psi_b = b/D_1 = 0.4, \cdots, 0.6$ for the open steel-textolite friction drives the following inequality guaranties the contact stress strength

$$a_{per} \ge 2(i-1)\sqrt[3]{\frac{KM_yE}{2fi\psi_b\,(0.418[\sigma_t])^2}}. \tag{25}$$

IV. PRECISION ANALYSIS OF THE STABILIZER

If, as it is inevitable in the real cases, the inertia ellipsoid of rotor varies from the exact sphere, or supporting frames do not provide an exact centering of the rotor, then the movement of the rotor obtains a qualitatively different and significantly more complex character.

The absolute motion of the rotor can be described as the sections of stationary rotation, which occur with a constant or constantly changing angular velocities; on the border of these sections practically the instantaneous change of the magnitude and the direction of the vector of angular velocity of the sphere $\omega_{ss}(t)$, corresponding to the impulse torque of the engines, occurs. The transfer from the absolute motion $\omega_{sa}(t)$ to the relative motion of the sphere ω_s can be obtained by

$$\omega_s = \omega_{sa} - \omega. \tag{26}$$

By writing down the motion equations of the rotor in the projections on its main central inertia axes $O'x'y'z'$, which are represented by the inertia moments I_1, I_2, I_3, generally assuming that are not equal, we will have

$$\begin{pmatrix} I_1\dot{\omega}_1 - (I_2 - I_3)\omega_2\omega_3 = M_x'' \\ I_2\dot{\omega}_2 - (I_3 - I_1)\omega_3\omega_1 = M_y'' \\ I_3\dot{\omega}_3 - (I_1 - I_2)\omega_1\omega_2 = M_z'' \end{pmatrix} \tag{27}$$

where $\omega_1, \omega_2, \omega_3$ are the projections of the angular velocities of the sphere $\boldsymbol{\omega}_s$ on the connected axes $O'x'y'z'$; M_x'', M_y'', M_z'', are the projections of the moment M_c' on the same axes.

Particularly, in the impulse control of motors and in the presence of perturbing moments $\boldsymbol{M}_p$ the rotor motion in the pauses between the impulses (e.i. when $\boldsymbol{M}_c' = 0$) does not coincide with the stationary rotating; vector $\boldsymbol{\omega}_s$, in this case does not remain fixed in relation to the rotor, but draws a complex curve on the surface of the inertia ellipsoid, changing its position with respect to axes $O'x'y'z'$ in a wide range.

However, in practice, there is no necessity to estimate the complex angular movement, occurred due to the inequality of its inertia moments I_1, I_2, I_3, because with the natural assumption

$$|I_1 - I_2|, \quad |I_2 - I_3|, \quad |I_3 - I_1| \ll I_1, \quad I_2, \quad I_3 \tag{28}$$

it affects the dynamics of the orientation system very weakly. In fact, the controlling moment $\boldsymbol{M}_c'$, produced by the stabilizer, corresponding with (13) does not depend evidently on the angular position of the rotor and depends (still in relatively weak order) just on the projections of its relative angular velocities p_s, q_s, r_s on the connected axes of the spacecraft $Oxyz$.

It is not difficult to establish that the fulfillment of the inequality (28) keeps the close compliance between vectors $\boldsymbol{\omega}_s$ and $\mathbf{H}$. In fact, using expressions

$$H'x = I_1\omega_x', \quad H'y = I_2\omega_y', \quad H'z = I_3\omega_z', \tag{29}$$

which contain the projections of vectors $\boldsymbol{\omega}_s$ and $\mathbf{H}$ on the axes $O'x'y'z'$, and supposing $I_1 > I_2 > I_3$, one can find that for the mismatch angle θ of the vectors $\boldsymbol{\omega}_s$ and $\mathbf{H}$ in the case of arbitrary disposition of these vectors relative to the axes $O'x'y'z'$ there occurs the inequality

$$0 \le (I_1 - I_2)/2I_3. \tag{30}$$

For a coefficient λ, relating to the vectors $\boldsymbol{\omega}_s$ and $\mathbf{H}$:

$$\lambda = \mathbf{H}/\boldsymbol{\omega}_s = \lambda(\omega_x',\ \omega_y',\ \omega_z') \tag{31}$$

with the same propositions we will have:

$$\lambda_{min} \le \lambda \le \lambda_{max},\ \lambda_{max}/\lambda_{min} = I_1/I_3. \tag{32}$$

With obtained estimations, for example, if $I_1 - I_3 = 0.01I_3$ the value of angle θ will be less than $20'$, and for the magnitudes λ_{max} and λ_{min}

$$\lambda_{max} = 0.01\lambda_{min}.$$

It follows that the measurement of the angular velocities ω_x, ω_y, ω_z allow predetermine correctly the kinetic moment of the stabilizer with accuracy within the indicated tolerances.

Since, further, the estimations (30) and (32) are applicable also to vectors $\boldsymbol{\omega}_s$ and $\mathbf{H}$ and in the case of the inequality (28) provide close accordance between them, the changes in the velocities ω_{xa}, ω_{ya}, ω_{za} (and consequently in ω_x, ω_y, ω_z), has to occur approximately as same, as in the case of exact equations

$$I_1 = I_2 = I_3 = I.$$

In other words, small differences of inertia moments of the rotor I_1, I_2, I_3 change the character of its angular movement qualitatively, but at the same time it has a weak effect on the angular velocity of the rotor $\omega_x(t)$, $\omega_y(t)$, $\omega_z(t)$, which have the main value in this case.

V. NUMERICAL EXAMPLE AND SIMULATIONS

A. NUMERICAL CALCULATION AND 3D DESIGN

The requirements, presented to the main parameters of a spherical stabilizer, e.g. weight, required energy, occupied space, and dynamical properties vary depending on the tasks which should be resolved by the attitude control system unit. The discussion of the election of some optimal parameters, for a particular satellite and task, needs a special study which is not the topic of this work.

In this section, as an example, we introduce the conceptual and structural design and analysis of a spherical stabilizer with the following parameters:

1) SPHERICAL SHELL ROTOR

- mass = 2 kg; diameter $D_s = 105$ mm; inertia moment $I_s \approx 0.016$ kg $\cdot$ m^2.

2) DC MOTORS

- Coreless, mass = 20 g; Power = 15 W; Output speed = 10000 rpm; torque $\tau_m = 0.015$ N·m.

3) TRANSMISSION PARAMETERS

- material: textolite-steel; transmission ratio $i = 5$; slip coefficient $\varepsilon = 0.01$; friction coefficient $f = 0.25$;
- diameter of driving wheels can be defined approximately using (17), then $D_1 \approx 21.2$ mm;
- width of the driving wheels $b = 0.4D_1 \approx 8.5$ mm.
- angular velocity of driving wheel $\omega_1 = \pi n/30 \approx 1050$ (1/s) and sphere $\omega_s = \omega_1/i \approx 210$ (1/s).

4) FORCE ANALYSIS

- effective force $F_t = \tau/D_1 \approx 0.7$ N; coupling reserve coefficient $K = 1.5$;
- necessary pressing force (from Eq. (18)), $F_p \approx 27.2$ N;
- permissible contact stress $[\sigma_t] = 60$ MPa; modulus of longitudinal elasticity (from Eq. (21)): $E = 0.19 \times 10^5$ MPa ($E_{textolite} = 0.1 \times 10^5$, $E_{steel} = 2 \times 10^5$ MPa);
- the value of interaxial distance a should satisfy the conditions stress condition (25): $a = D_1 + D_s = 126.2$ mm which is greater than the calculated permissible value $a_{per} = 0.01$ m.

5) TOLERANCES AND FITS

- referring to corresponding norms [32] the recommended assembly tolerance of the interaxial distance between the driving wheel and sphere in the active mode should be an interference fit *H8/u7*. This condition is obtained after the plastic deformation of the driving wheels.
- For the assembly of the spherical rolling elements and the rotor, using the same source [32] recommended fit is *L0/js6*.

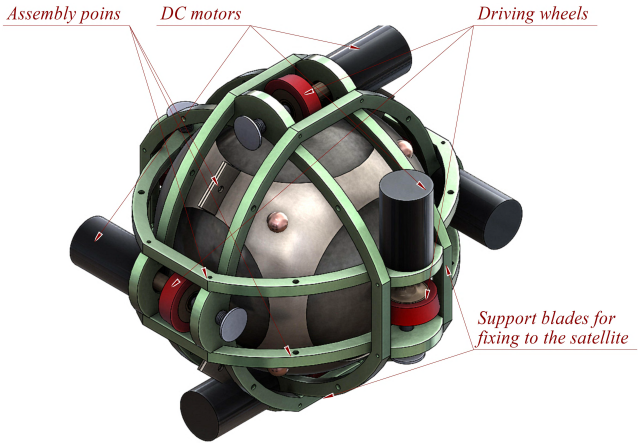

FIGURE 6. Schematic representation of the calculated spherical stabilizer.

In Fig. 6 the 3D model of the mechanism obtained by the above numerical example can be seen. The parallel frames and the spherical case can be connected to each other and then fixed to the satellite's body throw the connecting points.

From the presented example the size and power advantages of the proposed mechanism comparing to other spinning methods can be seen clearly. For instance, with piezoelectric actuator presented in [23] more power (45 W) is required to spin a lighter rotor (0.06) with a smaller rpm. A similar power property can be obtained using hysteresis method presented in [20] however, it has a big size disadvantage with its 1:19 rotor/total dimensional ratio.

B. FATIGUE ANALYSIS

To make sure that the designed mechanism performs efficiently during the operational life of a mission some individual numerical analysis are addressed in this subsection. The system is operating in the condition of repeated loading and unloading which may weaken some parts over time, even when the induced stresses are considerably, less than the allowable stress limits. Each cycle of stress fluctuation weakens the part to some extent and consequently after a number of cycles, the object becomes so weak that it fails. The fatigue of the driving wheels, due to its material and intensive condition of their operation, may, presumably, be the prime cause of the failure of the system and, therefore, will be studied in detail.

The driving wheels are subjected to different service environments and operating conditions during its life, starting

from the vibrations from the launch rockets to the harsh environmental conditions in space. The periodic contact stress during the active mode is far, the biggest load which can affect the body.

For the static stress study, we use the 3D model of the part brought from the assembly in Fig. 5 with the overall dimensions, obtained in the subsection V-A. The material of the wheels is textolite with the degree of filling of 60% material obtained by pressing at 20 MPa which has permissible contact stress $[\sigma_t] = 60$ MPa and modulus of elasticity equal to $E_e = 9 \times 10^3$ MN/m^2 [30].

To realize the analysis the Finite Element Method (FEM) in SOLIDWORKS Simulation is used. To define the fatigue analysis, as the basis, the result of a preliminary static study is needed. To obtain this, the von Mises stress method is used.

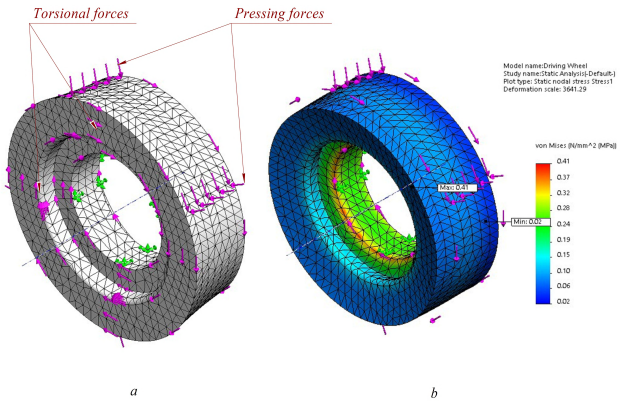

FIGURE 7. 3D design and static simulation of the driving wheel.

The following conditions are suggested (Fig. 7 *a*):

- The optimal solid mesh division of the model is obtained manually [33] and involves a total of 13,196 triangular elements and a total of 20665 nodes, Bearing loads in to be fixed elements and the;
- fixture on the internal cylindrical faces and restrained in the radial direction;
- Shrink fit contact set between the wheel and sphere with friction coefficient $f = 0.2$;
- deformation pressure created by the pressing forces $F_p = 27$ N due to the shrink fitting between the wheel and the sphere;
- transmitting torque $\tau_m = 0.015\text{N} \cdot \text{m}$ created by the DC motor and evenly applied around of the wheel.

Fig. 7, *b* shows the von Mises stress distribution on the surface obtained by the simulation. For a more visual model, the deformations are exaggerated. As it can be seen, the stress distribution is almost uniform in the entire part, except for some areas in the assembling hole. However, the stresses are very far (max = 0.41 MPa) from the yield strength limit of the body and are not destructible.

The results of the static simulations can now be used as the basis for defining a fatigue study. To realize the simulation following conditions are considered

- variable amplitude fatigue event due to the functioning conditions of the drive;
- frequency of the event = 3000 times (Estimated activation numbers of the wheels during the working life of a satellite);
- safety factor = 2;
- for fatigue failure to occur at a location depends on the material and the stress fluctuations which is provided by a curve called the fatigue stress (S) against the number of cycles to failure (N) curves, also known as Wöhler curve [34].

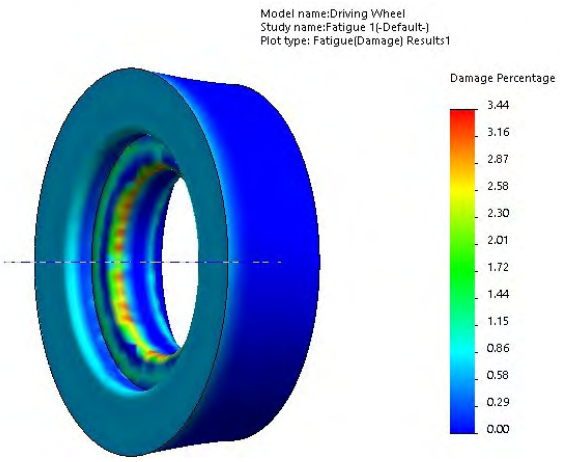

FIGURE 8. Failure percentage of the part during all the cycles.

The result of the fatigue analysis is depicted in Fig. 8. One can some cracks with the red color in the part which are basically caused as a result of repeated loading and unloading over time. However, the percentage of the possible failure is enough low which can guaranty the normal function of the transmission mechanism during the mission. To increase the number of cycles for a more long-lasting mission some improvements like the use of lubrication or a more resistant material might be the easiest solutions.

C. EXAMPLE OF SATELLITE CONTROL

To validate the effectiveness of the purposed controller, numerical simulations for attitude control of a microsatellite are presented here. The equations of angular motion of a satellite, containing a spherical stabilizer can be written as [25]:

$$\begin{aligned} J_x\ddot{\Omega}_x + J_* v_* \dot{\Omega}_y + \left(J_z - J_y\right) v_*^2 \Omega_x &= M_{px} - \dot{H}_x - v_* H_y \\ J_y\ddot{\Omega}_y - J_* v_* \dot{\Omega}_x + \left(J_z - J_x\right) v_*^2 \Omega_y &= M_{py} - \dot{H}_y - v_* H_x \\ J_z\ddot{\Omega}_z &= M_{pz} - \dot{H}_z \end{aligned} \tag{33}$$

where $\Omega_{x,y,z}$ are Euler angles, $J_{x,y,z}$ is the net inertia moment of the satellite without the sphere, $J_* = \left(J_x + J_y - J_z\right)$, v_* is the instantaneous orbital angular velocity directed along the opposite direction of the axis Oz_0 (Fig. 2).

As it can be seen from Eq. (33) the rotation angles in Ω_x and Ω_y (roll and yaw) are mutually connected, while the

rotation in the pitch (Ω_z), to a first approximation, can be considered as an independent. Therefore and for simplicity, we divide the control design of the system into two individual systems.

1) ROLL AND YAW CONTROL

The first two terms of satellite motion equations (33) can be expressed as

$$A_1\ddot{\boldsymbol{\Omega}} + A_2\dot{\boldsymbol{\Omega}} + A_3\boldsymbol{\Omega} = -\dot{\boldsymbol{H}} - B\boldsymbol{H} + \boldsymbol{M}_p, \tag{34}$$

where

$$\boldsymbol{\Omega} = \begin{pmatrix} \Omega_x \\ \Omega_y \end{pmatrix} \quad A_3 = \begin{pmatrix} (J_z - J_y)\, v_*^2 & 0 \\ 0 & (J_z - J_x)\, v_*^2 \end{pmatrix}$$

$$A_1 = \begin{pmatrix} J_x & 0 \\ 0 & J_y \end{pmatrix} \quad A_2 = \begin{pmatrix} 0 & J_* v_* \\ -J_* v_* & 0 \end{pmatrix}$$

$$\boldsymbol{H} = \begin{pmatrix} H_x \\ H_y \end{pmatrix} \quad B = \begin{pmatrix} v_* & 0 \\ 0 & v_* \end{pmatrix}$$

The system can be expressed in the space-state form as

$$\begin{aligned} \dot{\boldsymbol{x}}_1 &= \boldsymbol{x}_2, \\ \dot{\boldsymbol{x}}_2 &= f\,(\boldsymbol{x}_1, \boldsymbol{x}_2) + A_1^{-1}\boldsymbol{u} - \boldsymbol{\xi}, \end{aligned} \tag{35}$$

where

- $\boldsymbol{x}_1 = \boldsymbol{\Omega}, \boldsymbol{x}_2 = \dot{\boldsymbol{\Omega}} \in \Re^2$ are the state variables;
- $\boldsymbol{u} = -\dot{\boldsymbol{H}} - B\boldsymbol{H} \in \Re^2$ is the control input;
- $\boldsymbol{\xi} \in \Re^2$ represents the uncertainties affecting the system due to parameter variations, unmodelled dynamics (like friction, effect of slippage, etc.) and perturbations M_p;
- $f\,(\boldsymbol{x}_1, \boldsymbol{x}_2) = -A_1^{-1}A_2\boldsymbol{x}_1 - A_1^{-1}A_3\boldsymbol{x}_2$.

The spacecraft is chosen as similar in [35] with moment of inertias $J_x = 1.5$; $J_y = 0.651$, $J_z = 1.11\ 0 \cdot \mathrm{m}^2$. The spacecraft is supposed to move in a circular orbit at a height of 400 km with the angular velocity $v_* = 0.0011$ [rad/s].

Let us set a task to track some desired continuous and differentiable prescribed trajectory, i.e. $\mathbf{x}_1(t) \rightarrow \mathbf{x}_1^*(t)$, and consequently $\mathbf{x}_2(t) \rightarrow \mathbf{x}_2^*(t) = \dot{\mathbf{x}}_1^*(t)$. The controller must converge the error between actual and desired trajectories to zero in finite time in the presence of perturbation/uncertainties $\xi(t)$ (in simulation we take a perturbation equal to $0.5\sin(2t)$ and unmodeled dynamics equal to $(10\% \times \Omega_x)$.

Here we applied a recently proposed control laws based on *high-order continuous sliding mode control* (HOCSM) [36], [37]:

$$\begin{aligned} \mathbf{u}_{sm} - k_1 \lceil \mathbf{e}_1 \rfloor^{1/3} - k_2 \lceil \mathbf{e}_2 \rfloor^{1/2} + \eta \\ \dot{\eta} = -k_3 \lceil \mathbf{e}_1 \rfloor^0 - k_4 \lceil \mathbf{e}_2 \rfloor^0 \end{aligned} \tag{36}$$

where

$$\mathbf{e}_1(t) = \mathbf{x}_1(t) - \mathbf{x}_1^*(t), \quad \dot{\mathbf{e}}_1(t) = \mathbf{e}_2(t) = \dot{\mathbf{x}}_1(t) - \dot{\mathbf{x}}_1^*(t)$$

and the operator $\lceil \cdot \rfloor^\rho : \Re^n \mapsto \Re^n$, is defined component-wise as $\lceil \kappa \rfloor_i^\rho := |\kappa_i|^\rho sign\,(\kappa_i)$,

By choosing an appropriate constants $k_i, i = 1, \cdots, 4$ [37] the controller (36) stabilizes the system (35) to desired trajectories in finite time and in the presence of the perturbations/ uncertainties ξ.

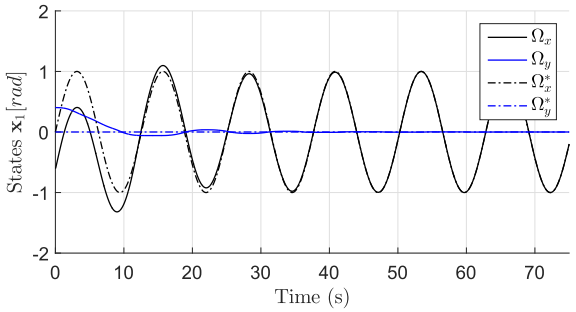

FIGURE 9. Tracking of roll and yaw angles.

The simulations in Figs. 9 and 10 show the tracking task of some desired continuous and differentiable prescribed trajectory: $\mathbf{x}_1^* = [sin(0.1t), 0]^\top$

Some of the main feathers of the proposed controller are [37]:

- The generated control signal is continuous;
- Lipschitz disturbances can be compensated;
- The states $\mathbf{x}_1$ and $\mathbf{x}_2$ converge to desired trajectories in finite time;
- The controller does not require for sliding variable designing, hence the controller design is simpler.

These properties may improve the quality of control in proposed system in which has many coefficients (e.g. friction and slip coefficients) which may easily change during the mission and affect the performance.

The required control inputs with chosen gains $k_i = [1.25, 17.88, 0.92, 0.44]$ are depicted in Fig. 11.[1]

2) CONTROL OF PITCH ANGLE

The task then in pitch can be chosen as

$$\Omega = \dot{\Omega} = 0 \quad \text{while } t \rightarrow 0$$

in the presence of perturbation/uncertainties.

From Eq. (33) the expression for movement of satellite in pitch angle can be expressed as

$$J_z\ddot{\Omega}_z = M_{pz} - \dot{H}_z. \tag{37}$$

With new variables

$$\Omega_z = \chi_1, \quad \dot{\Omega}_z = \chi_2,$$

and choosing the control variable as $w = -\dot{H}_z/J_z$, the perturbations as $\vartheta = M_{pz}/J_z$, the equation (37) can be rewritten as

$$\begin{aligned} \dot{\chi}_1 &= \chi_2, \\ \dot{\chi}_2 &= w + \vartheta. \end{aligned}$$

[1]Decomposition of the signals into $\mathbf{H}$ and $\dot{\mathbf{H}}$ and digitalization of this signal is not discussed in this work.

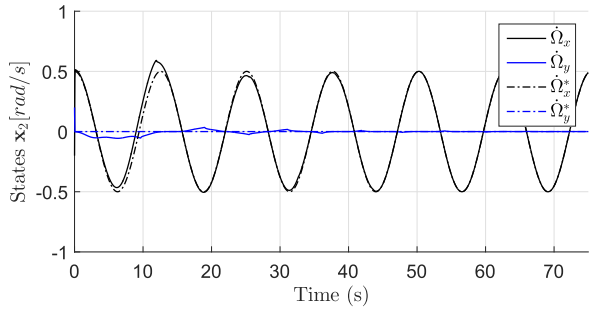

FIGURE 10. Tracking of angular velocities in roll and yaw by HOCSM controller.

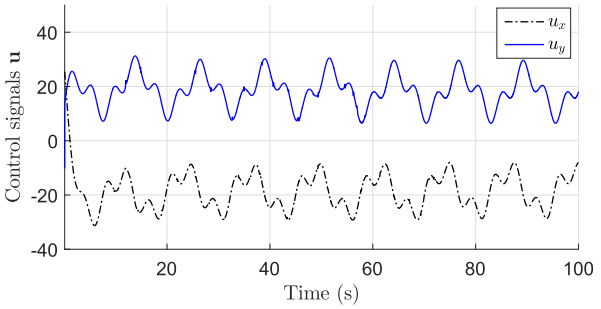

FIGURE 11. Control signals produced by HOSMC.

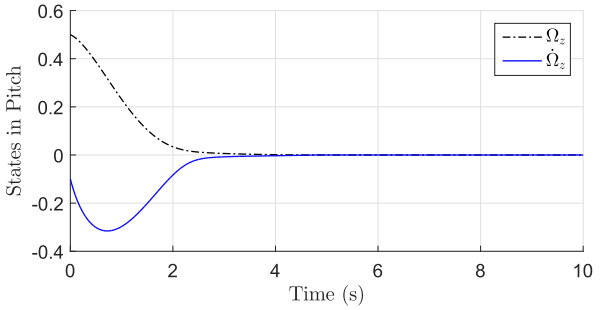

FIGURE 12. Angular position and velocity in pitch.

The similar controller structure as in Eq. (36) can be applied to provide a finite time convergence of the states χ_1 and χ_2 to zero while compensating perturbation ϑ.

$$\begin{aligned} w &= -\kappa_1 \lceil \chi_1 \rfloor^{1/3} - \kappa_2 \lceil \chi_2 \rfloor^{1/2} + \phi \\ \dot{\phi} &= -\kappa_3 \lceil \chi_1 \rfloor^{0} - \kappa_4 \lceil \chi_2 \rfloor^{0} \end{aligned} \tag{38}$$

Fig. 12 demonstrates that the convergence to origin with the perturbation equal to $2cos(0.5t)$ in the pitch direction can be reached in about 3 seconds. The control signal, With positive constants $\kappa_i = [13.7, 11.2, 2.4, 1.1]$, can be seen in Fig. 13.

D. DISCUSSION

A clear advantage of the presented mechanism compared with the popular pyramid type CMG (presented, as for an example, in the original work [35]), apart from size reduction, is the absence of singularity. As mentioned in the introduction, and also can be seen clearly from the Figs. 9 – 12, the regulation of the angular trajectories and velocities occur in a smooth trajectory created by the control torques presented in Fig. 11 and 13. With a pyramid type CMG system, however, there will be always some singularity surfaces which may affect the stabilization of the satellite [3], [35]. Although, as presented in [35], the singularities can be partially avoided by different control strategies, their complete elimination is not possible.

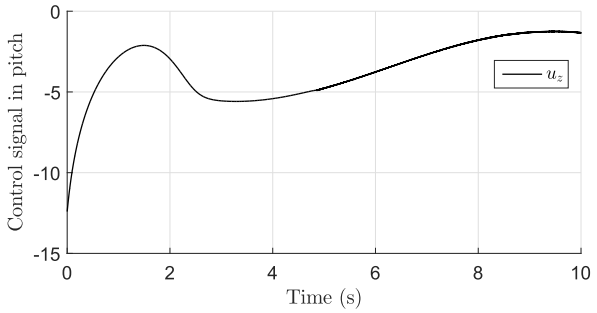

FIGURE 13. Control signal produced for orientation in the pitch direction.

The simplicity of the control algorithm of the proposed mechanism can be observed in the Eqs. (35) and (37) which are simulated in Figs. 11 and 13. The spherical stabilizer, in this case, is superior to other momentum exchange devices as double gimbal CMGs which have the disadvantages of mathematical complexity with implications for flight-software development and can also suffer from the is gimbal lock [3]. In the terms of simplicity, the proposed mechanism can be compared with the structure of the control torques created by a set of propulsion engines.

VI. CONCLUSIONS

The dynamic analysis and design concept of a new spherical stabilizer for small satellites is introduced. Detailed mathematical model and accuracy analysis of the mechanism is studied and an improved design concept for the friction drive of the mechanism is introduced. An example of a detailed design procedure is carried out which can be easily followed and proved. The numerical simulations are carried out to prove the fatigue analysis of the driving wheels of the transmission as well as the performance of the controller as an attitude control device.

REFERENCES

[1] M. N. Sweeting, "Modern small satellites-changing the economics of space," *Proc. IEEE*, vol. 106, no. 3, pp. 343–361, Mar. 2018.
[2] K. B. Chin *et al.*, "Energy storage technologies for small satellite applications," *Proc. IEEE*, vol. 106, no. 3, pp. 419–428, Mar. 2018.
[3] F. A. Leve, B. J. Hamilton, and M. A. Peck, *Spacecraft Momentum Control Systems*. Cham, Switzerland: Springer, 2015.
[4] F. L. Markley and J. L. Crassidis, *Fundamentals of Spacecraft Attitude Determination and Control*, S. T. Library, Ed. New York, NY, USA: Springer, 2014.
[5] H. Kojima, K. Hiraiwa, and Y. Yoshimura, "Experimental study on line-of-sight (LOS) attitude control using control moment gyros under microgravity environment," *Acta Astron.*, vol. 143, pp. 118–125, Feb. 2018.

[6] H. Kojima, "Calculation and fitting of boundaries between elliptic and hyperbolic singularities of pyramid-type control moment gyros," *Acta Astron.*, vol. 104, no. 1, pp. 33–44, 2014.
[7] S. Kwon, T. Shimomura, and H. Okubo, "Pointing control of spacecraft using two sgcmgs via LPV control theory," *Acta Astron.*, vol. 68, nos. 7–8, pp. 1168–1175, Apr./May 2011.
[8] R. Takehana, H. Paku, and K. Uchiyama, "Attitude control of satellite with a spherical rotor using two-degree-of-freedom controller," in *Proc. 7th Int. Conf. Mech. Aerosp. Eng. (ICMAE)*, Jul. 2016, pp. 352–357.
[9] H. Kojima, P. Trivailo, and Y. Yoshimura, "Spacecraft line of sight maneuver control using skew-arrayed two single-gimbal control moment gyros," *Trans. Jpn. Soc. Aeronautical Space Sci. Jpn.*, vol. 14, no. ists30, pp. Pd_31–Pd_37, Apr. 2016.
[10] V. J. Lappas, W. H. Steyn, and C. Underwood, "Design and testing of a control moment gyroscope cluster for small satellites," *J. Spacecraft Rockets*, vol. 42, no. 4, pp. 729–739, 2005.
[11] D. J. Richie, V. J. Lappas, and G. Prassinos, "A practical small satellite variable-speed control moment gyroscope for combined energy storage and attitude control," *Acta Astron.*, vol. 65, pp. 1745–1764, Dec. 2009.
[12] W. Haeussermann, "The spherical control motor for three axis attitude control of space vehicles," NASA, Washington, DC, USA, Tech. Rep. X-50071, 1959.
[13] J. Spitzer, Jr., "Space telescopes and components," *Astron. J.*, vol. 65, no. 5, pp. 242–263, 1960.
[14] K. Tanaka, Y. Tsuda, T. Saiki, Y. Shirasawa, and R. Jifuku, "The development of the spherical aerostatic bearings for 3DRW," in *Proc. 21st Workshop JAXA Astrodyn. Flight Mech.*, 2011, p. 2014.
[15] D.-K. Kim, H. Yoon, W.-Y. Kang, Y.-B. Kim, and H.-T. Choi, "Development of a spherical reaction wheel actuator using electromagnetic induction," *Aerosp. Sci. Technol.*, vol. 39, pp. 86–94, Dec. 2014.
[16] F. Da, F. Chunshi, and S. Jian, "An inductive reaction momentum sphere system," China Patent 104 143 947, Sep. 21, 2016.
[17] F. Chunshi, F. Dahe, Y. Zhangnan, L. Xiaoyun, and S. Jian, "Modularized fast aggregatable reaction sphere," China Patent 2015 10 860 492, Mar. 9, 2016.
[18] L. Rossini *et al.*, "Development and closed-loop experimental results of a reaction sphere elegant breadboard," in *Proc. 16th Eur. Space Mech. Tribol. Symp.*, Bilbao, Spain, Sep. 2015, pp. 1–6.
[19] E. Stagmer, "Reaction sphere for stabilization and control in three axes," U.S. Patent 9 475 592 B2, Oct. 25, 2016.
[20] L. Zhou, "Magnetically suspended reaction sphere with one-axis hysteresis drive," Ph.D. dissertation, Dept. Mech. Eng., Massachusetts Inst. Technol., Cambridge, MA, USA, 2014.
[21] W. Haeussermann, "Space vehicle attitude control mechanism," U.S. Patent 3 017 777, Jan. 23, 1962.
[22] L. Zhu, J. Guo, and E. Gill, "Review of reaction spheres for spacecraft attitude control," *Prog. Aerosp. Sci.*, vol. 91, pp. 67–86, May 2017.
[23] H. Paku and K. Uchiyama, "Satellite attitude control system using a spherical reaction wheel," *Appl. Mech. Mater.*, vol. 798, pp. 256–260, Oct. 2015.
[24] V. Bakanauskas, R. Bansevičius, D. Bručas, and A. Domeika, "Development of a novel device for attitude control over small satellites," *Solid State Phenom.*, vol. 220, pp. 561–564, Jan. 2015.
[25] S. Keshtkar, J. A. Moreno, H. Kojima, K. Uchiyama, M. Nohmi, and K. Takaya, "Spherical gyroscopic moment stabilizer for attitude control of microsatellites," *Acta Astron.*, vol. 143, pp. 9–15, Feb. 2018.
[26] E. Buchoud *et al.*, "Enhancement of an optical fiber sensor: Source separation based on brillouin spectrum," *IEEE Access*, vol. 1, pp. 789–802, 2013.
[27] B. V. Raushenbakh and E. N. Tokar, *Attitude Control of Spacecrafts*. Moscow, Russia: Nauka, 1974.
[28] E. A. Avallone, T. Baumeister, III, and A. Sadegh, *Marks' Standard Handbook for Mechanical Engineers*, 11th ed. New York, NY, USA: McGraw-Hill, 2006.
[29] R. G. Budynas, J. K. Nisbett, and J. E. Shigley, *Shigley's Mechanical Engineering Design*, 10th ed. New York, NY, USA: McGraw-Hill, 2015.
[30] B. K. Sharma, *Industrial Chemistry* (Including Chemical Engineering). New Delhi, India: GOEL Publishing House, 1997.
[31] Y. Ni *et al.*, "Superior mechanical properties of epoxy composites reinforced by 3D interconnected graphene skeleton," *ACS Appl. Mater. Interfaces*, vol. 7, no. 21, pp. 11583–11591, 2015.
[32] *Geometrical Product Specifications (GPS)—ISO Code System for Tolerances on Linear Sizes—Part 2: Tables of Standard Tolerance Classes and Limit Deviations for Holes and Shafts*, Standard 286-2:2010(en), International Organization for Standardization, Geneva, Switzerland, 2010.
[33] P. Kurowski, *Engineering Analysis With SOLIDWORKS Simulation*. New York, NY, USA: SDC Publications, 2017.
[34] P. Strzelecki and T. Tomaszewski, "Analytical models of the S-N curve based on the hardness of the material," *Procedia Structural Integrity*, vol. 5, pp. 832–839, Sep. 2017.
[35] H. Kojima, "Singularity analysis and steering control laws for adaptive-skew pyramid-type control moment gyros," *Acta Astron.*, vol. 85, pp. 120–137, Apr./May 2013.
[36] J. A. Moreno, D. Y. Negrete, V. Torres-González, and L. Fridman, "Adaptive continuous twisting algorithm," *Int. J. Control*, vol. 89, no. 9, pp. 1798–1806, 2016.
[37] V. Torres-González, T. Sanchez, L. M. Fridman, and J. A. Moreno, "Design of continuous twisting algorithm," *Automatica*, vol. 80, pp. 119–126, Jun. 2017.

SAJJAD KESHTKAR received the bachelor's and M.Sc. degrees in aerospace engineering from the Kharkov Aviation Institute, Ukraine, in 2009 and 2011, respectively, and the Ph.D. degree in automatic control from Cinvestav-IPN, Mexico, in 2016. He is currently with the School of Engineering and Science, Tecnológico de Monterrey, Mexico. He does research in mechanism and machine design and automatic control of complex and nonlinear mechanical systems and their application in aerospace industry.

JAIME A. MORENO was born in Colombia. He received the Ph.D. degree *(summa cum laude)* in electrical engineering (automatic control) from Helmut-Schmidt University, Hamburg, Germany, in 1995, the Diploma degree in electrical engineering (automatic control) from the Universität zu Karlsruhe, Karlsruhe, Germany, in 1990, and the Licentiate degree (Hons.) in electronic engineering from Universidad Pontificia Bolivariana, Medellin, Colombia, in 1987. He is currently a full Professor of automatic control and the Head of the Electrical and Computing Department, Instituto de Ingeniería, Universidad Nacional Autónoma de México, Mexico. He is the author and editor of eight books, four book chapters, one patent, and author and co-author over 300 papers in refereed journals and conference proceedings. His current research interests include robust and nonlinear control with application to biochemical processes, the design of nonlinear observers and higher order sliding mode control. He is a member of the Technical Board of IFAC.

HIROHISA KOJIMA (M'05) received the B.E., M.E., and Ph.D. degrees from the Department of Aeronautics and Astronautics, The University of Tokyo. He is currently a Professor with the Department of Aerospace Engineering, Tokyo Metropolitan University. His current research interests are dynamics and control of space robots, optimization, and chaos control. He is a member of JSASS, JSME, SICE, and RSJ, and a Senior Member of the AIAA. He was an Associate Editor of *Inverse Problems in Science and Engineering* and *The Open Aerospace Engineering Journal*. He is on the Editorial Board of the *International Journal of Space Science and Engineering*.

EUSEBIO HERNÁNDEZ received the bachelor's degree in electronic engineering from the Technological Institute of Celaya, Mexico, in 2002, the master's degree in instrumentation and automatic control from the Autonomous University of Querétaro (UAQ), Mexico, in 2004, and the Ph.D. degree in mechanical engineering from UAQ and the University of Cassino, Italy, in 2010. He was a Visiting Scholar with the University of Cassino in 2008 and 2009. He is currently a Professor with the Instituto Politécnico Nacional, ESIME Ticoman, Mexico. His research focuses on simulation, robotics and mechanisms, with specific interest in kinematics, optimized design, and error modeling of parallel robots.